Journal of Controlled Release 384 (2025) 113848

Contents lists available at ScienceDirect

Journal of Controlled Release

journal homepage: www.elsevier.com/locate/jconrel

Direct structural investigation of pH responsiveness in mRNA lipid nanoparticles: Refining paradigms

Christoph Wilhelmy [a], Lukas Uebbing [a], Bastian Kolb [a], Melissa A. Graewert [b], Thomas Nawroth [a], Heinrich Haas [a,*], Peter Langguth [a,*]

[a] Department of Biopharmaceutics and Pharmaceutical Technology, Johannes Gutenberg-University, Mainz, Germany
[b] European Molecular Biology Laboratory, Hamburg Outstation, Hamburg, Germany

ARTICLE INFO

Keywords:
Messenger RNA
Lipid nanoparticle
LNPs
SAXS
Ionizable lipids
Structure-function correlation

ABSTRACT

Using small angle X-ray scattering measurements, structural coherencies in lipid nanoparticle (LNP) formulations comprising messenger RNA (mRNA) were elucidated in response to pH changes and as a function of RNA to lipid ratio. Formulations were assembled using selected ionizable lipids with well-known activity from previous experiments, with otherwise identical composition. Several structural parameters were determined, including internal organization, fraction of ordered material, the underlying repeating distance, and the fractal dimension of the overall particles. Repeat distances increased with increasing pH, with profiles similar to the shape of pK_a curves, therefore allowing to directly reveal the structural implication of the pH responsiveness inside the particles. The fractal dimension, which so far had not been in the center of attention for quality control, was correlated with biological activity. Such systematic data on structure-function coherencies in LNPs can serve as complementary methods to standard lab-based quality control measures. This can help to facilitate and accelerate the rational formulation development of new RNA therapeutics.

1. Introduction

For the application of messenger RNA (mRNA) in pharmaceutical products, delivery systems tailored for the intended route of application and therapeutic intervention are required [1–5]. Since the authorization of the first RNA-based therapies, with applications in gene silencing therapy [6] and as vaccines for SARS-CoV-2 [7], so-called lipid nanoparticles (LNPs) have become a focal point of interest. These consist, besides the nucleotide cargo, of a specific mixture of four lipids, with an ionizable lipid being a key element for functionality [5,8,9].

Despite the broad interest, many aspects of LNPs related to their activity and quality remain elusive to the developer community. A few generally accepted concepts or paradigms exist, such as regarding the optimum pK_a value of the ionizable lipid [10], or the capacity to undergo lamellar to hexagonal phase transitions [11,12]. However, these are more conceptual than precise directives for selecting suitable systems.

So far, the development of novel delivery systems largely relies on screening lipids, lipid compositions, and the lipid to RNA ratio (known as N/P ratio) [2,13–15]. However, this process can be tedious and time-consuming because of the vast number of potential combinations, along with the risk that not all highly active compositions are recognized. Here, we pursue an approach to identify structural aspects of LNPs that correlate with activity, to provide a knowledge base for better experimental planning towards improved formulations.

One parameter of interest is the pK_a value of the ionizable lipid, which gives information on how the charge of the ionizable lipid changes with pH. It is considered relevant for the efficacy of endosomal escape [16,17]. The pK_a is typically determined by a fluorescence assay using the dye molecule 6-(p-toluidino)-2-naphthalenesulfonic acid (TNS). This process involves the binding of the dye and a change in fluorescence intensity as a function of the lipid's ionization state within the particle [10]. It should be noted that the pK_a value determined by this fluorescence assay is strongly affected by the local environment in the LNP. It differs substantially from that of one of the free ionizable lipid molecules in solution, which is typically much higher [18]. Therefore, it is frequently referred to as the apparent pK_a value.

Although not supported by all experimental data, it is widely accepted that an apparent pK_a value between 6 and 7 is most appropriate for optimal LNP activity. Jayaraman and colleagues stated that a pK_a of

* Corresponding authors.
E-mail addresses: haashein@uni-mainz.de (H. Haas), langguth@uni-mainz.de (P. Langguth).

https://doi.org/10.1016/j.jconrel.2025.113848
Received 14 March 2025; Received in revised form 12 May 2025; Accepted 14 May 2025
Available online 20 May 2025

6.2 to 6.5 is ideal for siRNA delivery to the liver [16]. Hassett et al. published that the optimal pK_a for immunogenicity after intramuscular administration is between 6.6 and 6.8 [19], which led to the development of the SM-102 lipid used in the Spikevax® vaccine. Despite this, the pK_a of the ionizable lipid ALC-0315 used in the Comirnaty® vaccine is reported as 6.09 [20], but it also led to comparable therapeutic results.

This highlights that the apparent pK_a of the LNP determined by the aforementioned method does not always allow for an exact prognosis of potential therapeutic efficiency, without even considering differences among tested cell types and routes of administration [21]. Notwithstanding these unresolved issues, it seems clear that the ability to measure and control the pK_a value is an essential tool for tailoring nanoparticles. For example, it has been shown that by adding a fifth component, the so-called selective organ targeting (SORT) molecule, to the LNP formulation, selectivity towards lung or spleen was achieved, with the apparent pK_a of the formulation being shifted towards higher or lower values [22].

While the TNS assay is a straightforward lab-based method, the obtained apparent pK_a values are highly influenced by experimental conditions such as buffer choice and varying dye sensitivity at extreme pH values [23], which impairs the comparability of results obtained from different laboratories and systems. A general limitation of the fluorescence assay is that it detects only the lipids accessible to the dye from the bulk phase, which does not necessarily reflect the properties of the overall particle. An alternative method to estimate the pK_a of an LNP formulation involves computational techniques that allow for estimation from the lipid structures [24]. Other approaches include molecular dynamics simulations to study pH-driven phase transitions and to determine the actual pK_a inside the LNP formulation [25]. However, although these approaches deliver promising results, they require further verification through comparison with more experimental data.

Here, we applied an approach to directly determine pH-dependent changes in the structural properties of the overall particle using small angle X-ray scattering (SAXS) measurements [26]. In extensive previous SAXS and small angle neutron scattering (SANS) studies [26–30], we revealed several fundamental structural features of mRNA nanoparticles and demonstrated the influences of manufacturing protocols, lipid composition, and polymer grafting on structure and functionality [29,31,32]. By tracking lamellar spacing and other structural parameters as a function of pH in multilamellar model systems, we obtained curves similar in shape to pK_a curves, allowing us to determine the structural analogue of the pK_a value, denominated as structural pK_a.

In the present measurements, we investigated the pH responsiveness of LNPs containing a series of ionizable lipids, namely DODAP, DODMA, Dlin-MC3-DMA (MC3), and ALC-0315, using SAXS measurements. The relative activity of formulations based on the respective ionizable lipids is well-known from several previous studies, which describe potency both in vitro and in vivo [18,33,34]. Based on that, we further classified these model lipids with increasing potency in the order given above. We revealed the structural characteristics of the different systems, including their type of internal organization (lamellar or hexagonal), the repeating distance of the ordered material, and overall particle organization, expressed as the fractal dimension. LNPs from lipids with higher biological activity shared certain structural properties. These insights may lead to refined paradigms for quality evaluation of LNP formulations and criteria for tailoring future mRNA delivery systems.

2. Materials and methods

2.1. Materials

1,2-dioleoyl-sn-glycero-3-ethanolamine (DOPE) was manufactured by Lipoid GmbH (Ludwigshafen, Germany). 1,2-dioleyloxy-3-dimethylaminopropane (DODMA), N-palmitoyl-sphingosine-1-{succinyl [methoxy(polyethylene glycol)2000]} (C16-PEG2000-Ceramide), and Cholesterol were manufactured by Avanti Polar Lipids (Alabaster, AL, USA). DODAP (1,2-dioleoyl-3-dimethylammonium-propane), (6Z,9Z,28Z,31Z)-heptatriacont-6,9,28,31-tetraene-19-yl-4-(dimethylamino) butanoate (DLin-MC3-DMA) and ALC-0315 ([(4-Hydroxybutyl) azandiyl]bis(hexan-6,1-diyl)bis(2-hexyldecanoat)) was purchased from MedChemExpress (Monmouth Junction, NJ, USA). mRNA encoding for eGFP was purchased from etheRNA (Niel, Belgium). 6-(p-toluidino)-2-naphthalenesulfonic acid (TNS), KH_2PO_4, and Na_2HPO_4 were obtained from Sigma-Aldrich (St. Louis, MO, USA), and glycylglycine was obtained from Carl Roth (Karlsruhe, Germany).

2.2. LNP preparation

LNPs were prepared using a dedicated ethanol injection method developed by our group as described earlier [31]. The mRNA was diluted to the intended concentration with a 10 mM aqueous glycylglycine solution (pH 5.7 ± 0.1), and the ethanolic lipid stock solutions were pre-mixed to obtain the targeted molar ratios (Table 1). The aqueous mRNA buffer was pipetted onto the lipid mix, and the sample was then immediately vortexed for 10 s. This single-step protocol allows for the manufacturing of mRNA LNPs in a directly applicable buffer without further modification. The LNPs manufactured with this protocol exhibit larger sizes than those obtained with microfluidic mixing (about 200 nm compared to 100 nm) but were described to be comparable in in vitro and in vivo potency and show similar structural features [32]. Therefore, particularly regarding the structural features observed here, we expect the results to be equally applicable for microfluidically manufactured mRNA LNPs.

All LNPs comparing different ionizable lipids were prepared at a molar ratio of ionizable lipid to mRNA (N/P ratio) of 5:1. For the N/P ratio variation, LNPs between N/P 0.2 and N/P 5 were formulated. Molar ratios were calculated as 100 mol% = $\sum$ mol% (helper lipid, ionizable lipid, cholesterol, stealth moiety). The LNP composition can be seen in Table 1.

2.3. Dynamic light scattering (DLS)

The samples were diluted to an appropriate concentration (1 mg/mL total lipid for size, 0.1 mg/mL for zeta potential) in glycylglycine buffer and then transferred to a Zetasizer Nano ZS (Malvern Panalytical Ltd., UK) for size measurements using dynamic light scattering (DLS) and zeta potential determination. The DLS measurements were conducted as backscattering measurements (scattering angle: 173°) at 25 °C after a 30 s equilibration time. Results are presented in Supplementary Table 1.

2.4. Small-angle X-ray scattering (SAXS)

Data were obtained at the P12 BioSAXS beamline of the European Molecular Biology Laboratory (EMBL) at the PETRAIII synchrotron, located at DESY (Hamburg, Germany) [35]. The experiments were performed with an X-ray energy of 10 keV ($\lambda = 0.124$ nm) at a 3.0 m sample detector distance, resulting in a q range of ~0.03–7 nm^{-1}. Samples had a total lipid concentration of 2.5 mg/mL. Using the BioSAXS automatic sample changer [36], 30 µL of the sample was transferred to a quartz capillary mounted in vacuum, where the sample was exposed 20 times for 0.095 s to the beam. The scattering intensity was collected by a Pilatus 6M detector (Dectris, Baden, Switzerland). The buffer of each sample was measured under the same conditions before and after each sample run for buffer subtraction. For the investigations on LNP pH responsiveness, the samples were mixed with phosphate buffer as proposed by Sörensen [37] from pH 4.5 to 10 for samples with N/P < 1 and from pH 4.5 to 8 for samples with N/P > 1. Aqueous solutions of KH_2PO_4 and Na_2HPO_4 at 150 mM were mixed in different ratios, and the pH was adjusted with 0.1 M HCl or NaOH. Samples were mixed with phosphate buffers immediately before the SAXS measurements, and the pH was checked. The ATSAS 3.0 software package (EMBL Hamburg, Germany) was used for averaging of repeated measurements

Table 1
Composition of investigated mRNA LNPs.

Formulation	Ionizable Lipid	Ion. Lipid [mol%]	DOPE [mol%]	Cholesterol [mol%]	Stealth lipid [mol%]	mRNA [mol%]
DODAP N/P 5	DODAP	40	10	48	2	8
DODMA N/P 5	DODMA	40	10	48	2	8
MC3 N/P 5	DLin-MC3-DMA	40	10	48	2	8
ALC-0315 N/P 5	ALC-0315	40	10	48	2	8
DODMA N/P 0.2	DODMA	1.6	48.4	48	2	8
DODMA N/P 0.65	DODMA	5.2	44.8	48	2	8
DODMA N/P 2	DODMA	16	34	48	2	8
DODMA N/P 4	DODMA	32	18	48	2	8
MC3 N/P 0.2	DLin-MC3-DMA	1.6	44.8	48	2	8
MC3 N/P 0.65	DLin-MC3-DMA	5.2	44.8	48	2	8
MC3 N/P 2	DLin-MC3-DMA	16	34	48	2	8
MC3 N/P 4	DLin-MC3-DMA	32	18	48	2	8

and buffer subtraction [38]. Subtracted data were further analyzed using QTIPlot 1.0.1 (IONDEV Sr, Bucuresti, Romania), as described in the following section.

All scattering data are given as scattering intensity I as a function of the momentum transfer, q, calculated according to eq. (1), with 2θ being the scattering angle and λ the X-ray wavelength.

$$q = \frac{4\pi}{\lambda}\sin\left(\frac{2\theta}{2}\right) \tag{1}$$

SAXS data for the investigated q-range include the form factor of the single lipid nanoparticles, which is determined by the overall size, shape, and surface properties of the nanoparticles, as well as Bragg reflections derived from mRNA-lipid interactions as part of their internal structure.

Determination of the intensity decay of the SAXS pattern can reveal information about the shape and (surface) fractal dimension of the nanoparticles. Using the power law shown in Eq. (2), the Porod exponent, D, is determined.

$$I(q) = I_0 \cdot q^{-D} \tag{2}$$

Scattering from ideally smooth interfaces is characterized by a Porod exponent of 4 (Porod law [39]), while a value of 2 indicates a diluted Gaussian chain, and a slope of −1 points towards rigid rods. Of interest here are the intermediate values, which reflect the surface roughness. By using eq. (3), the surface fractal dimension, D_s, is obtained [40]. For ideally smooth surfaces, D_s is 2, while with rising value (between 2 and 3), the surface roughness increases [41]. Values above 3 are indicative of conformations of polymers in solution, as stated above.

$$D_s = 6 - D \tag{3}$$

For investigations of internal structure properties, Lorentzian fit functionality was used for peak fitting in the SAXS pattern, as given in eq. (4)

$$\mathrm{I(q)} = \mathrm{I_0} + \frac{2\mathrm{A}}{\pi}\cdot\frac{\mathrm{w}}{4\cdot(\mathrm{q}-\mathrm{q_c})^2 + \mathrm{w}^2} \tag{4}$$

where I_0 is the baseline intensity, A the area under the peak, w the peak width at half maximum (FWHM), and q_c the peak center position (Supplementary Table 2). The peak is derived from the ordered mRNA-lipid complexes [26,30], where from the position of the peak center, the repeat distance (d-spacing) is obtained by the Bragg eq. (5)

$$d = \frac{2\pi}{q_c} \tag{5}$$

The peak width, w, provides information about the extent of the ordered stacks [42], which can be described by the correlation length, ξ. In the model for liquid crystalline structures [43] correlation length, ξ, is calculated by Eq. (6), which is defined as the distance at which the positional correlation decays to the value 1/e:

$$\xi = \frac{2}{\mathrm{w}} \tag{6}$$

For formulations with an N/P ratio > 1, for the Bragg peak, Lorentzian fits with two overlaying peaks were used according to eq. (7)

$$\mathrm{I(q)} = \mathrm{I_0} + \frac{2\mathrm{A_1}}{\pi}\cdot\frac{\mathrm{w_1}}{4\cdot(\mathrm{q}-\mathrm{q_{c_1}})^2 + \mathrm{w_1}^2} + \frac{2\mathrm{A_2}}{\pi}\cdot\frac{\mathrm{w_2}}{4\cdot(\mathrm{q}-\mathrm{q_{c_2}})^2 + \mathrm{w_2}^2} \tag{7}$$

For the determination of the structural pK_a of the LNP formulations, a Boltzmann fit was used to describe the sigmoidal evolution of d-spacing as a function of pH and to determine the inflection point of the function as in eq. (8)

$$d-spacing = d-spacing_{max} - \frac{d-spacing_{max} - d-spacing_{min}}{1 + 10^{\frac{pKa-pH}{pH}}} \tag{8}$$

Where d-$spacing_{max}$ and d-$spacing_{min}$ are the upper and lower limits of the fit, and pK_a is the inflection point of the function, which is taken as structural pK_a.

2.5. pK_a fluorescence assay

A common previously published assay using the fluorescent dye 2-(p-toluidino)-6-naphthalene sulfonic acid (TNS) was performed to determine the apparent formulation pK_a [44]. Measurements were performed in triplicate on black TC-coated 96-well plates, with each well containing 10 μL sample (at 0.1 mg/mL total lipid), 90 μL buffer (phosphate buffer as proposed by Sörensen from pH 4.5 to pH 10 [37]) and 2 μL of TNS in DMSO (300 μM). The fluorescence was measured from the top on a TECAN Infinite 200Pro plate reader (Tecan Group Ltd., Männedorf, Switzerland) at 325 nm excitation and 435 nm emission wavelength. Apparent pK_a of the formulation was determined using a sigmoidal Boltzmann fit,

$$NFI = NFI_{max} - \frac{NFI_{max} - NFI_{min}}{1 + 10^{\frac{pKa-pH}{pH}}} \tag{9}$$

where NFI_{max} and NFI_{min} are the maximal and minimal normalized fluorescence intensity, and pK_a is the inflection point of the fit, which is stated as the apparent pK_a of the formulation.

3. Results

3.1. Comparison of ionizable lipids

We investigated mRNA LNPs bearing four different ionizable lipids (DODAP, DODMA, MC3, and ALC-0315; Table 1, Fig. 1A) under otherwise identical conditions. For manufacturing, we used a proprietary protocol (see Methods and Materials), which does not require complex equipment, and has proven to result in particles with equivalent biological activity. As determined by comparative studies, we assume the

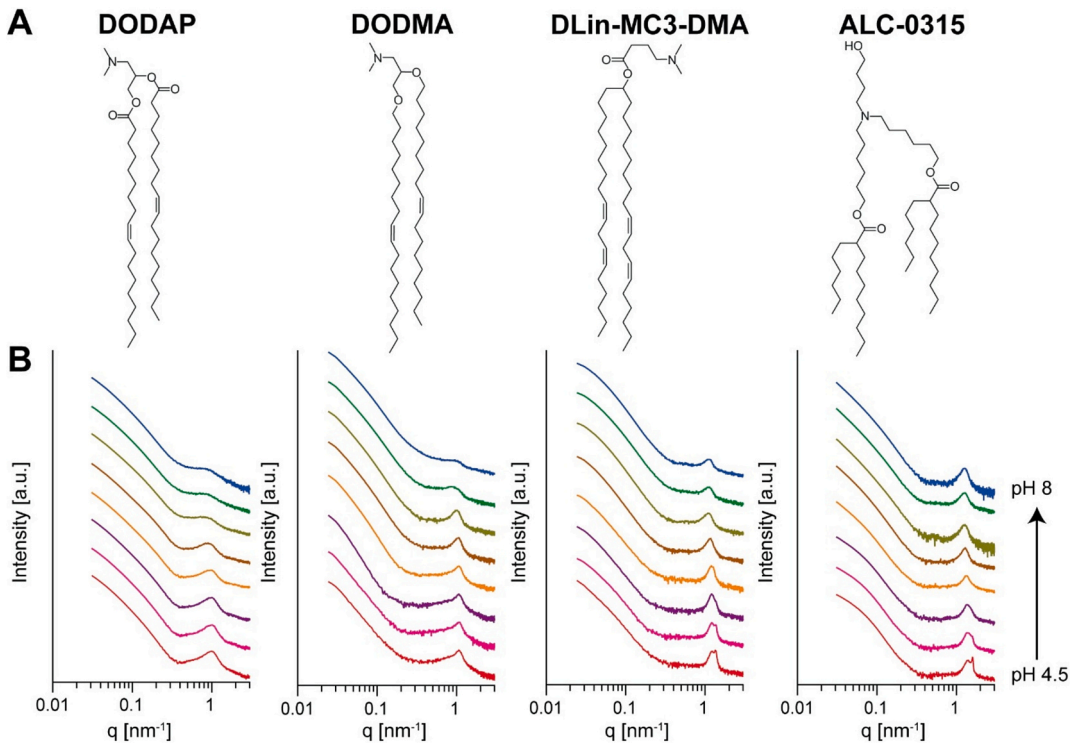

Fig. 1. SAXS measurements for mRNA-LNPs with different ionizable lipids (from left to right: DODAP, DODMA, DLin-MC3-DMA, ALC-0315): A. Structure of the used ionizable lipids in the order mentioned above. B. SAXS curves of mRNA-LNP samples over a pH range from 4.5 (red curves, bottom) to pH 8.0 (dark blue curves, top) in ΔpH = 0.5 steps. In all cases, phosphate buffers were used for pH adjustment. The SAXS curves are shifted on the logarithmic y-axis for better visualization. (For interpretation of the references to colour in this figure legend, the reader is referred to the web version of this article.)

particles to be equivalent in internal structure to LNPs, which are produced with microfluidic approaches [32]. Based on previous studies, the relative potency of these model lipids is well-known, where activity is assumed to increase in the above-mentioned order. The samples' size determination by Dynamic Light Scattering (DLS) revealed average sizes between 170 and 210 nm with a polydispersity index around 0.2, and Zeta-Potentials between 19 and 30 mV for all formulations (see Supplementary Table 1).

To gain insight into structural changes during manufacturing and to mimic the behavior of the LNPs after administration, SAXS measurements were conducted as a function of bulk phase pH. These conditions reflect the transition from near-neutral pH during circulation in the bloodstream to stepwise acidification during endosomal uptake, leading to acidic pH in late endosomal processing [45].

All SAXS patterns shared some common features, including smooth curves with a steep decay in intensity up to a q-value of approximately 0.4 nm^{-1} and a pronounced peak resulting from Bragg reflections of ordered material. For all formulations, the Bragg peak position shifted towards lower q-values (increase of d-spacing) with increased pH. This shift was accompanied by a decrease in the area and a broadening of the peak, where for DODAP and DODMA-LNPs, the peak was barely visible at pH 8 (Fig. 1B). The Bragg peaks originated from repeating lipid and mRNA stacks, consisting of only a very low number of repeating units [26,29,30]. As observed in previous studies, we found indications for the presence of two types of ordered lipid material (e.g., with high and low amounts of mRNA inserted) having slightly different repeat distances. Therefore, we fitted the Bragg reflections using a double Lorentzian function and determined the peak position, peak width, and peak area of each peak. While for the high-q (lower d spacing) peak of the two Bragg peaks, the position decreased with an increasing pH, the second peak, at a lower q-value (higher d spacing), showed only minor changes or even increased for MC3- and ALC-bearing LNPs. Additionally, the area of the peak at higher q-values decreased with increasing pH, while the area of the low-q peak either remained unchanged or increased with increasing pH (Fig. 2). We conclude that the low-q peak derived from lipidic substructures with little or no mRNA content, while the high-q peak originates from mRNA/lipid stacks and is further referred to as the main peak. Additionally, for MC3 and ALC-0315, a third, very sharp peak, corresponding to a repeat distance of about 4 nm, was visible at low pH, which diminished with increasing pH and disappeared above pH 5.5 (Supplementary Fig. 1). Partial phase separation of the lipid mixture, leading to the formation of domains (e.g., rafts) with specific repeat distances, may be the reason for this observation. These results highlight the complexity of the LNPs as pharmaceutical products. Multiple fractions with varying structures and pH-dependence may coexist in the same particles or in the form of different particle populations.

For the main peak, resulting from repeating lipid bilayers with mRNA inserted in the hydrophilic head group regions, the pH dependence of the d-spacing arises from the electrostatic interactions between mRNA and lipids. At acidic pH, the ionizable lipid reaches its highest level of protonation, resulting in the strongest electrostatic attraction with the negatively charged mRNA and, thus, the lowest repeat distance. As the pH increases, the ionizable lipid's protonation level decreases, and the negative charge of mRNA is no longer completely balanced by positive lipid charges. This results in weakening of the attraction forces between mRNA and lipid, and thus, increased repeat distances, and a loss of order. Therefore, the position of the main peak shifted to lower q, the width increased (indicative of a loss of correlation length), and its area decreased as pH increased. For the secondary peak, which corresponds to a higher repeat distance, we expect either a lower amount of mRNA or none to be inserted between the repeating layers. In that case, the reduction of the lipid protonation state with an increase in pH results in a reduction of the repulsive interaction between the adjacent layers, consistent with the observed trend for a decrease in the repeat distance (Fig. 2). The large excess of ionizable lipid in relation to the mRNA (N/P 5) makes segregation into fractions of different composition and

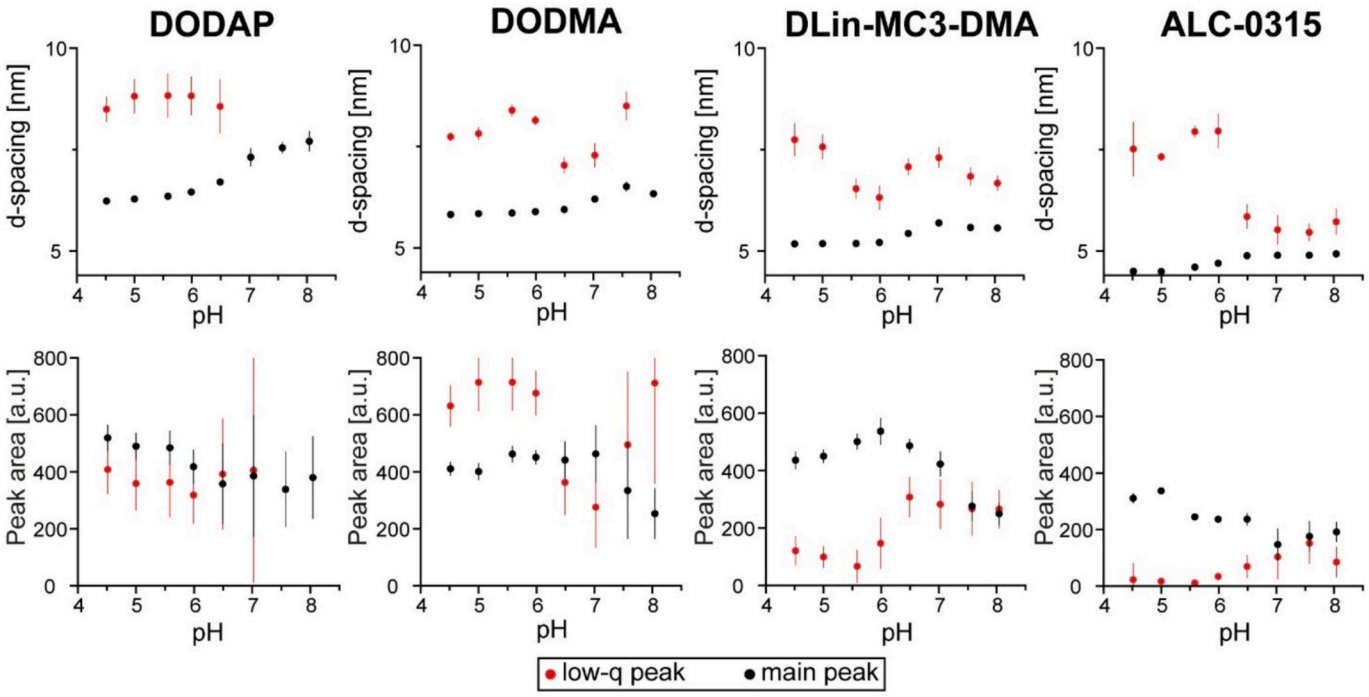

Fig. 2. d-spacing and peak width from both peak fractions. As determined by double-peak Lorentzian fitting, d-spacing (top), and peak area (bottom) of the low-q peak (red) and the main Bragg peak (black) are displayed as a function of pH. Note that for DODAP over pH 7, no low-q peak was detectable due to overlay with intensity decay in the Porod region, and at pH 8, the low-q d-spacing exceeds the scale of the graph.

structure plausible. It is important to note that from the batch SAXS measurements presented here, it is difficult to determine whether the different patterns coexisted in the same particles, or whether different particle populations having the respective structure were present. For a clearer answer, fractionation of the particles based on size, surface charge, or other characteristics before the SAXS measurements would be beneficial. For example, coupling of asymmetrical flow field flow fractionation to SAXS (AF4-SAXS) has successfully been applied to combine a size separating technique with structure analysis for investigation of lipoplexes and LNPs [28,46].

The observations were in accordance with previous findings on multilamellar model systems with and without mRNA [26]. Similar to the above conjectures, multilayers without mRNA displayed decreasing d-spacing with increasing pH, while in the presence of mRNA, the d-spacing increased. Here, we were able to determine such pH-dependent effects for the situation in LNPs, which are of higher practical interest but are more complex and less defined, due to the intrinsically lower degree of order and the coexistence of different characteristic structures.

The pH dependence of the d-spacing for the main peak was analyzed using a Boltzmann formalism (see Methods section). The inflection points of the sigmoidal curves were taken as the structural pK_a and compared to the apparent pK_a, derived from the fluorescence-based assay (Fig. 3A, Table 2). Interestingly, for DODMA and MC3-LNPs, the apparent pK_a determined by the TNS assay (Table 2, Supplementary Fig. 2) showed comparable values to the SAXS-based approach, whereas differences were observed for LNPs composed of DODAP and ALC-0315. While the apparent pK_a of DODAP-LNPs was lower than the structural pK_a, for ALC-0315-LNPs, it was the opposite.

Several structural aspects of the systems derived from different ionizable lipids showed correlation with their activity [18,33,34]. The overall d-spacing of the LNP formulations manufactured from lipids with higher activity showed lower d-spacings than the LNPs made with low activity ionizable lipids (Fig. 3A, Supplementary Table 3). At pH 4.5, the value for DODAP-LNPs was almost 2 nm higher than that for ALC-0315, even though the ALC-0315 lipid possesses a bulkier structure than DODAP. As well, the total shift of d-spacing was lower for the LNPs comprising high activity ionizable lipids (Fig. 3A). While for DODAP-LNPs the increase of the repeat distance was 1.45 nm, for LNPs with MC3- and ALC-0315 it was only about 0.5 nm.

In addition to changes in peak position, we observed differences in peak area and width as a function of pH (Supplementary Fig. 3). The peak area diminished for all tested formulations as the pH increased. The peak width increased for the systems manufactured with the two less active lipids (DODAP and DODMA), resulting in a decrease in correlation length as pH increased. The higher activity MC3- and ALC-0315-LNPs did not show such an effect (Fig. 3B). When investigating the organization of the ordered stack, depicted as the ratio of correlation length to repeating distance, particularly for ALC-0315-containing LNPs, no loss of spatial order within the tested pH range was observed (Supplementary Fig. 4). Therefore, the loss of order with increasing pH is lower for active LNPs than for those with less active lipids.

Another property correlated with activity is the Porod exponent, D. It is derived from a power law analysis of the intensity decay by fitting a function based on eq. (2) to the experimental curve between the Bragg peak and the Guinier region. For scattering from an ideally smooth interface, the intensity decays with the fourth power of q ($I(q) \sim q^{-4}$) [39]. Real interfaces exhibit a certain roughness, which, in this case, results from the distribution of molecular moieties perpendicular to the interface. This leads to decreasing values for D as surface roughness increases. There are several ways to express the surface roughness. In a general mathematical approach, instead of the Porod exponent, the (interfacial) fractal dimension, D_s, is observed (see eq. (3)) [29,47].

D_s has a value of 2 for ideal interfaces, and up to $D_s = 3$, increasing surface roughness is deduced. Values for D_s higher than 3 are better represented by a model of a Gaussian (polymer) chain conformation [40,41]. In earlier studies, a higher biological activity was observed for LNPs with higher surface fractal dimension [31]. Here, further to that previous finding, we observed that LNPs prepared with three higher activity ionizable lipids showed an increase in surface fractal dimension upon pH decrease, while the low activity ionizable lipid DODAP exhibited no change across the entire pH range (see Fig. 3C). Notably, the pH at which the LNPs reorganize towards a higher fractal dimension

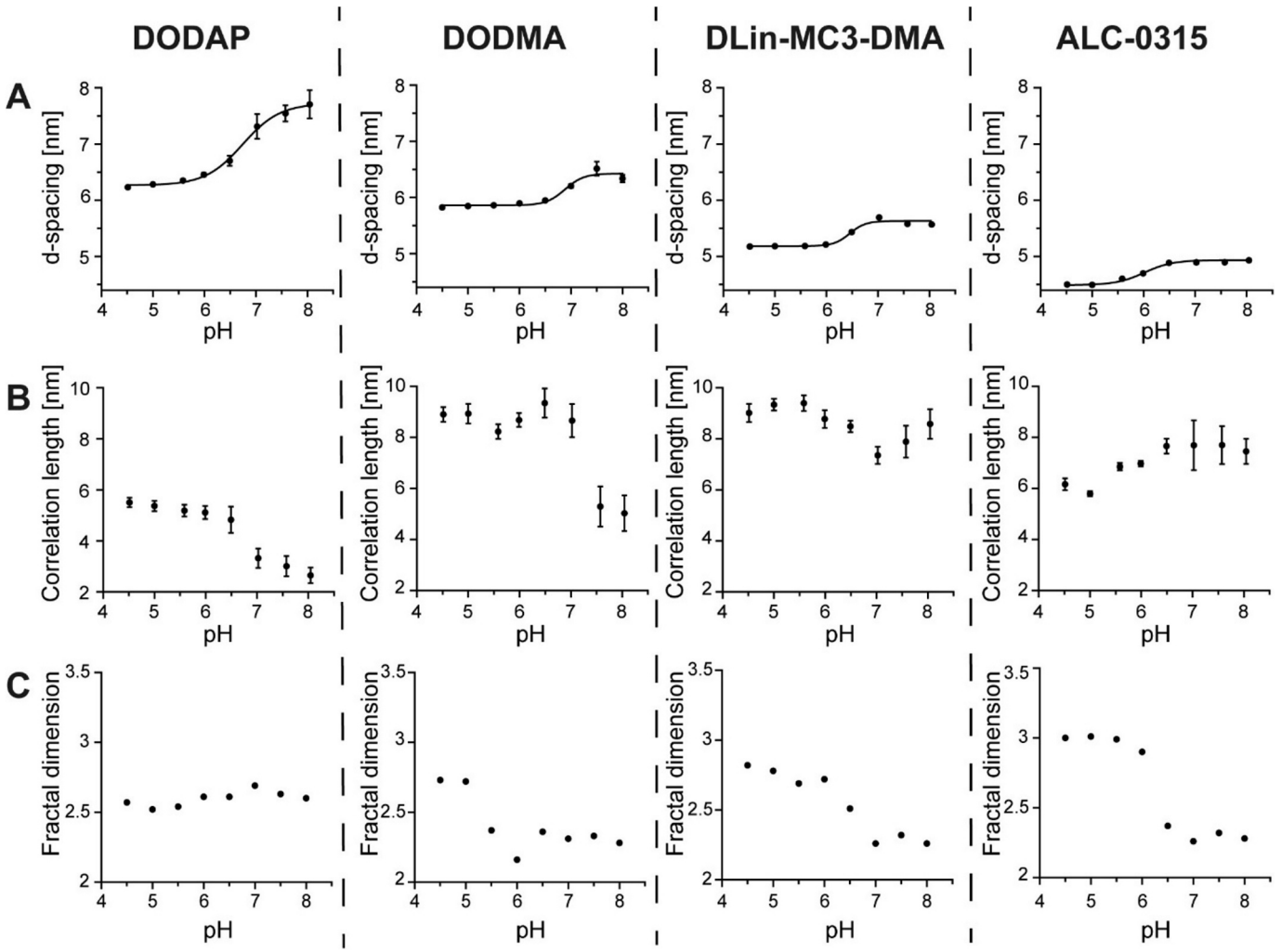

Fig. 3. Analysis of SAXS derived parameters as a function of pH. A. Values for d-spacing calculated by the peak position as described in the methods section (see Eq. (5)) as a function of environmental pH. The black line indicates a sigmoidal fit, whose inflection point can be used as the structural pK_a. B: Correlation length as a function of pH, calculated from the peak width (FWHM). While DODAP and DODMA LNPs show a decrease in correlation length, the more potent lipids maintain their long-range order. C. Fractal dimension from analysis of lower q-range (<0.4 nm^{-1}) using a power law as a function of surrounding pH. Values of 2 indicate smooth surfaces, whereas with growing values, the surface roughness increases.

Table 2
Results of determination of the structural pK_a by SAXS and the apparent pK_a by TNS assay for the investigated mRNA LNP with varying ionizable lipids.

Formulation	SAXS structural pK_a	TNS apparent pK_a
DODAP N/P 5	6.7 ± 0.1	5.8 ± 0.1
DODMA N/P 5	6.9 ± 0.2	6.6 ± 0.1
MC3 N/P 5	6.5 ± 0.1	6.7 ± 0.2
ALC-0315 N/P 5	6.0 ± 0.1	6.7 ± 0.1

differs from the structural pK_a. Differences in changes of internal structure, as indicated by d-spacing, and surface roughness in response to pH changes may be related to a different lipid composition in the LNP surface layer [48]. Interestingly, among the tested ionizable lipids, the ALC-0315 LNPs show the highest fractal dimension and therefore the highest surface roughness at low pH values.

Certain general structural differences between high and low activity LNPs observable over the total pH range were identified. While for the LNPs from the less active lipids, DODAP and DODMA, Bragg peak areas for main and secondary peaks were similar, for MC3 and ALC-0315 the main peak takes ~75 % of the additive total peak area for MC3 and even ~95 % of the total area for ALC-0315 at acidic pH (Fig. 2). This would mean that monophasic formulations tend to have higher activity, while the presence of a second structure, either as an mRNA-poor phase in the particles or an RNA-poor particles population, would point towards lower activity.

As a general observation, we note that slight molecular structure changes can substantially affect overall organization. The two less active lipids, DODAP and DODMA, which only differ by an ether-to-ester substitution (see Fig. 1A), exhibited clearly different d-spacings, with DODMA showing smaller values. It still needs to be clarified if, in this case, it has consequences for biological activity, but it highlights the potential impact of even small molecular changes on LNP properties.

In summary, compared to less potent formulations, LNPs manufactured with highly potent ionizable lipids, such as MC3 and ALC-0315, showed (i) lower overall d-spacing, (ii) a reduced range of d-spacing changes as a function of pH, (iii) no loss of long-range order with increasing pH, and (iv) a pH dependent change in surface roughness, with high fractal dimensions especially at low pH values.

3.2. *Variation of N/P ratio*

To further explore the structural organization properties of LNP formulations, SAXS measurements were conducted on formulations with

varying lipid to mRNA ratios (N/P ratios) for two selected ionizable lipids: the less active DODMA and the more active MC3. The N/P ratio is a critical formulation parameter that determines the quality and activity of LNPs. In standard screening approaches, functional N/P ratios are to be found empirically, as, so far, no direct molecular rationale for determining appropriate N/P ratios is available. In this study, we screened a wide range of N/P ratios, including conditions of mRNA excess (N/P < 1). Such low N/P ratios are of particular interest, since nanoparticle formulations assembled at N/P < 1 have proven high selectivity for spleen targeting upon intravenous injections [2], and products on this basis are currently undergoing different stages of clinical trials for cancer immunotherapy [49]. Formulation parameters are provided in Table 1. The total lipid concentration was kept constant to generate comparable experimental conditions, so that only the ionizable and helper lipid fractions were varied to set the N/P ratio.

Size determination by DLS exhibited a trend towards an increase in LNP size with decreasing N/P ratio. Samples manufactured with an excess of mRNA showed negative Zeta-potentials, while those manufactured with a lipid excess were positively charged in the acidic manufacturing buffer (Supplementary Table 1).

SAXS patterns of LNPs were recorded as a function of bulk phase pH, covering the range from 4.5 to 10 for LNPs with an N/P ratio < 1, and from 4.5 to 8 for LNPs with N/P > 1 (Fig. 4). The overall characteristics of the curves for the samples were similar to those described above. Also, for the additionally tested N/P ratios, a shift of peak position towards lower q-values (as displayed by the d-spacing in Fig. 5A), peak broadening, and a decrease of peak area were observed with increasing pH. Notably, all formulations manufactured at an N/P ratio < 1 exhibited only one peak pattern, with a narrow first-order Bragg peak and additional higher-order peaks (Supplementary Fig. 5), mainly detectable in acidic environmental buffers. Therefore, in contrast to the situation at N/P> > 1, only a single type of ordered material with a high degree of organization was present. A clearly higher correlation length (lower peak width) was determined, likely because the order is not disturbed by a second fraction of material (Fig. 5B). The positions of the higher-order peaks correspond to $\sqrt{3}$ and 2 times the q-value of the first-order peak (Supplementary Table 4), indicative of a hexagonal liquid-crystalline organization [50,51]. It was shown before that ionizable lipids can undergo lamellar to hexagonal phase transition upon acidification, which appears to be beneficial for the potency of the respective lipids [12]. Favorable conditions for the hexagonal packing found here can also include the increased content of DOPE within formulations with a decreasing N/P ratio in our experiments (see Materials and Methods). Due to its cone-like shape, with small headgroup and bulky unsaturated hydrocarbon chains, DOPE is known to readily undergo lamellar to hexagonal phase transition [8,51,52].

We assume that for formulations manufactured with an excess of mRNA, the nanoparticles consist of repeating stacks of lipid-complexed mRNA with fixed stoichiometry, where excess mRNA is present as free molecules in the bulk phase. Such patterns were observable up to an N/P ratio of 2. Only at higher N/P ratios did the secondary low-q peak emerge, which is indicative of the mRNA-depleted structural motif. With increasing N/P ratio, the relative area of the secondary peak shows a trend to increase (Supplementary Fig. 6), in accordance with increasing amounts of mRNA-poor ordered material.

The overall d-spacing and the range of d-spacing within the pH spectrum varied for the tested formulations (Fig. 5A, Supplementary Table 5). The d-spacing under acidic conditions, such as in the state of

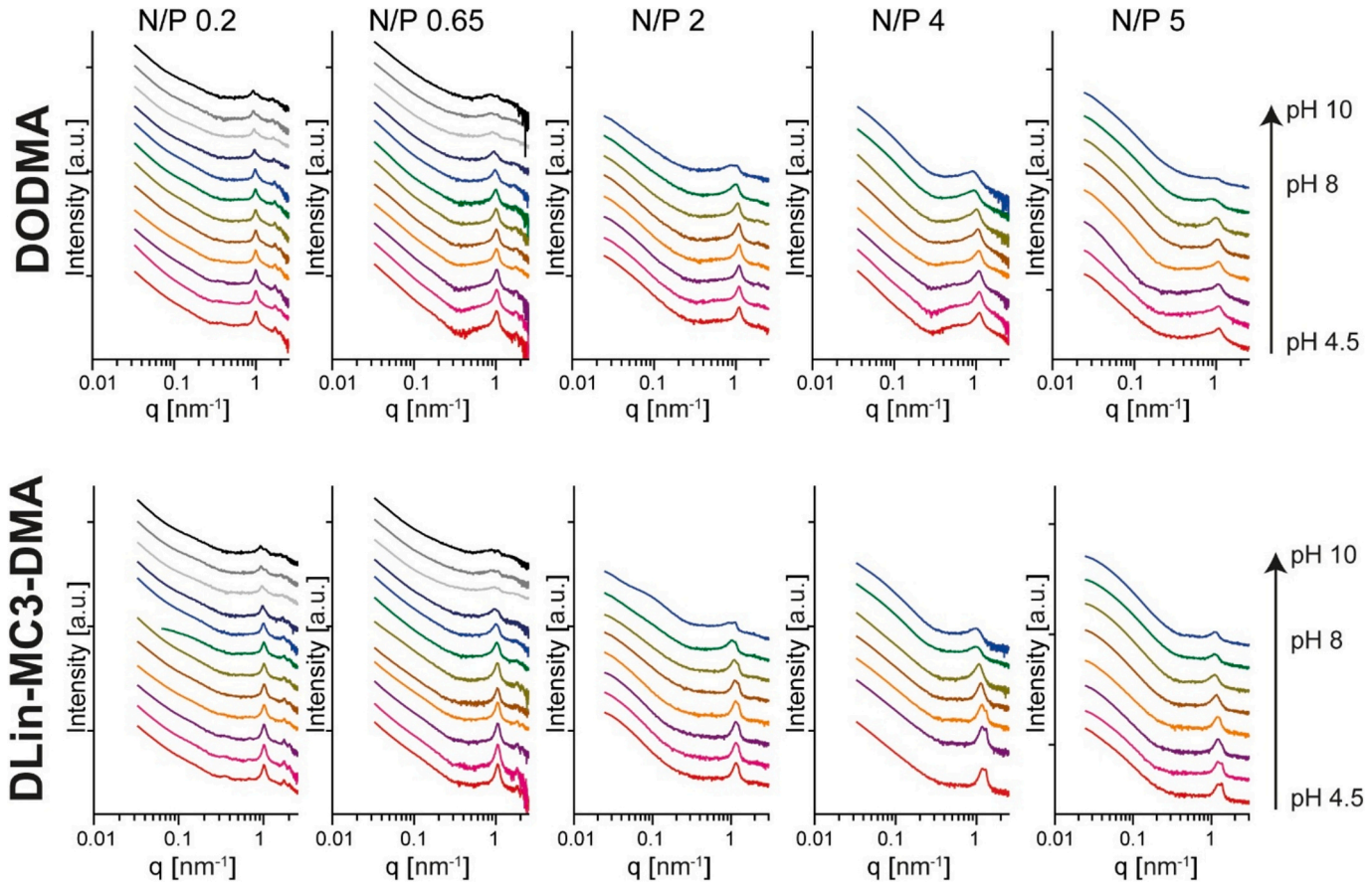

Fig. 4. Results of SAXS measurements of LNPs with N/P ratio variations. SAXS curves of mRNA-LNP samples over a pH range from 4.5 (red curves, bottom) to pH 10 (black curves, top) or to pH 8(blue curves, in case N/P ratio > 1) in ΔpH = 0.5 steps. The visualization of pH-dependent structure evolution is similar to that of LNPs described in Fig. 1B. (For interpretation of the references to colour in this figure legend, the reader is referred to the web version of this article.)

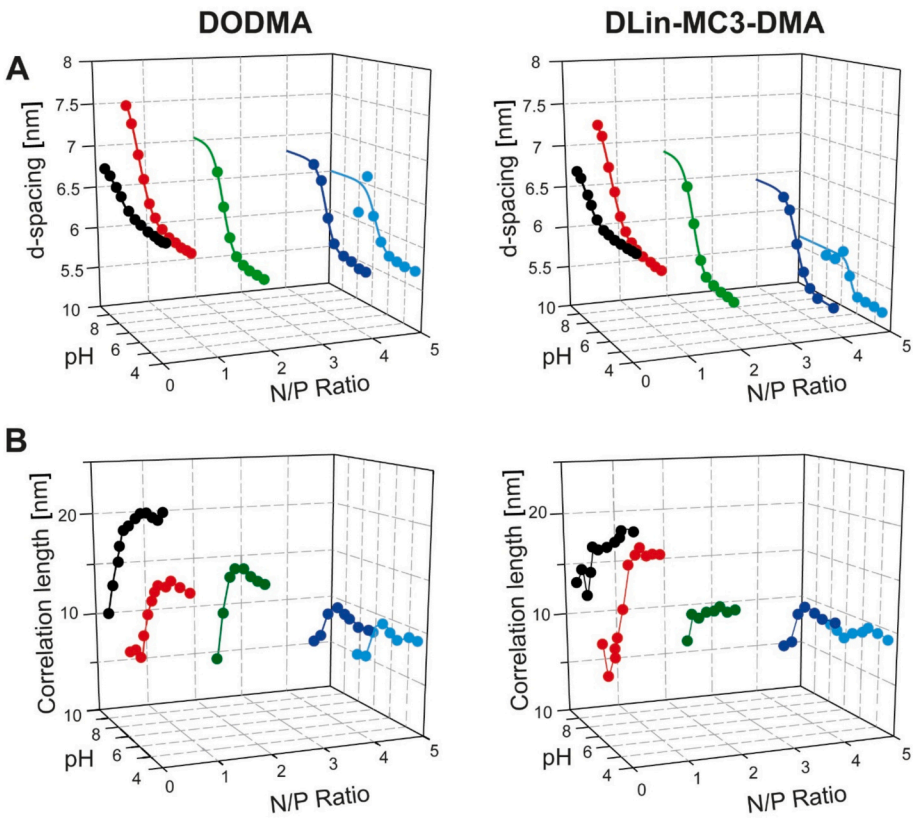

Fig. 5. Results of peak analysis for DODMA (left) and MC3 (right) LNPs of varying N/P ratio (black: N/P 0.2, red: N/P 0.65, green: N/P 2, dark blue: N/P 4, light blue: N/P 5). A: d-spacing of all LNPs as a function of pH value (z-axis) and N/P ratio (x-axis). Sigmoidal fits were added as described before. For LNPs with an N/P ratio > 1, fits were extrapolated to pH 10 for illustration. B: Correlation length of all LNPs as a function of pH and N/P ratio. (For interpretation of the references to colour in this figure legend, the reader is referred to the web version of this article.)

full protonation, decreased with increasing N/P ratio, indicating a higher packing density of the mRNA/lipid stacks. In most LNP formulations, N/P ratios at the higher end of this range are selected, which, according to the results observed here, are characterized by tighter mRNA complexation. Regardless of whether there is a direct correlation between packing density and activity, such structural information can provide a quantitative basis for identifying quality-relevant properties of LNP drug products.

When analyzing the structural pK_a for a given formulation, we observe a clear dependence on the N/P ratio (Table 3). The structural pK_a shifted from about 8.5 to about 6.5 on increasing the N/P from 0.2 to 5. Therefore, this dependence of the pK_a value on the N/P ratio may be applied as a valuable tool for fine-tuning LNP properties with a given ionizable lipid. In fact, also in the fluorescence-based assay, a shift towards higher apparent pK_a was visible for formulations with decreasing N/P ratio but revealing higher discrepancies to the structural pK_a with decreasing N/P ratio (Fig. 6). The controlled variation of the pK_a value has been demonstrated earlier with formulations having optimized organ targeting properties using the SORT technology [22]. By adding a fifth, charged lipid to the LNP, a clear effect on the pK_a value was obtained. At the same time, organ targeting towards the spleen or the lung was improved. This underlines the potential of accurate control of the

Table 3
Results of the determination of structural pK_a by SAXS and apparent pK_a by fluorescence-based TNS assay of the formulations tested for N/P ratio variation.

Formulation	SAXS structural pK_a	TNS apparent pK_a
DODMA N/P 0.2	8.6 ± 0.2	8.3 ± 0.2
DODMA N/P 0.65	8.7 ± 0.1	7.8 ± 0.2
DODMA N/P 2	7.7 ± 0.1	7.5 ± 0.3
DODMA N/P 4	7.2 ± 0.1	6.9 ± 0.1
DODMA N/P 5	7.0 ± 0.2	6.6 ± 0.1
MC3 N/P 0.2	8.6 ± 0.1	7.4 ± 0.2
MC3 N/P 0.65	8.6 ± 0.1	7.6 ± 0.1
MC3 N/P 2	7.7 ± 0.1	7.1 ± 0.1
MC3 N/P 4	7.0 ± 0.1	6.7 ± 0.1
MC3 N/P 5	6.5 ± 0.1	6.7 ± 0.2

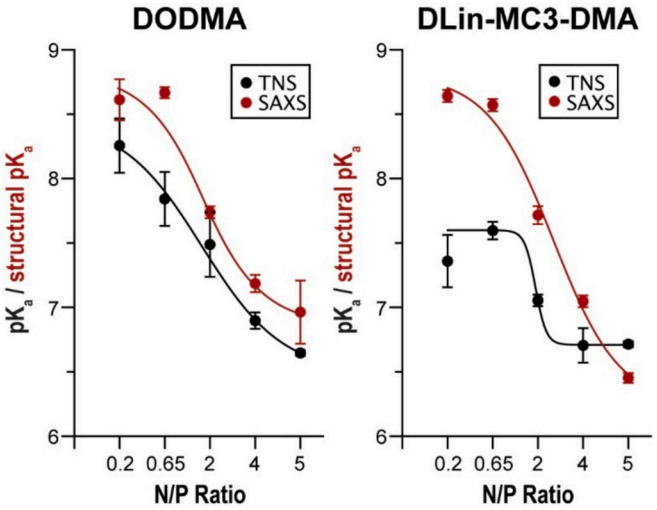

Fig. 6. Apparent pK_a (black, as determined with TNS-assay) and structural pK_a (red, as determined by SAXS analysis) as a function of N/P ratio of the LNP formulations. Lines were added for both parameters for illustration purposes. (For interpretation of the references to colour in this figure legend, the reader is referred to the web version of this article.)

pH responsiveness of the nanoparticles for tailoring their biological activity.

Also, distinct observations were made when looking at the fractal dimension of the particles in the extended range of N/P variation. The fractal dimensions of the LNPs with N/P < 1 were even higher than 3, therefore indicating a conformation more similar to a polymeric chain rather than 'only' elevated surface roughness [41]. We hypothesize that in LNPs assembled at N/P < 1, part of the excess mRNA forms shell-like structures at the surface of the particles, where it also accounts for the negative zeta potential. The conformational organization of the mRNA, essentially being a high molecular weight biopolymer, is responsible for the experimentally measured high fractal dimension. Increasing pH and therefore decreasing electrostatic interactions between the LNP and the RNA layer further foster this phenomenon at mRNA excess (Supplementary Fig. 7). For high N/P formulations (N/P ratio 4 and 5), the absolute fractal dimensions were lower but increased with decreasing pH value for both tested lipids. Considering the low pH in the late endosome, these findings on surface organization may be of relevance also for the efficacy of mechanisms involved in endosomal release.

Taken together, quantitative structure analysis, such as done here by SAXS measurements, provides valuable information on how the N/P ratio influences the internal structural organization, surface properties, as well as the pH-dependent behavior of LNPs. The N/P ratio directly impacts the pH responsiveness, highlighting the potential of N/P ratio variation as a tool for LNP fine-tuning. This complexity should be considered for rational development of mRNA LNP formulations.

4. Discussion

Control strategies are of essential importance for the assessment of the quality of LNP products. They are required during the development of new formulations, as well as for regular quality control and stability evaluation of existing products. Structural information plays a central role in product quality evaluation. SAXS measurements are a powerful tool for determining various structural parameters of LNP formulations at different length scales, ranging from Angstroms to several hundred nanometers. For application in pharmaceutical practice, it is important to quantitatively analyze data, using standardized protocols to allow for better comparability between results from different laboratories and systems. Based on this, generally accepted criteria need to be defined to evaluate product quality.

As a result of the present study, we can suggest a set of defined and quantitative structural parameters to be considered in SAXS data analysis of LNP and similar formulations. For the scattering profiles, Bragg peak analysis should include determination of position, width, and area, with a decision on whether single or double peak fitting is appropriate. Observation of structural features as a function of pH is important for several reasons. Firstly, this reflects the pathway during manufacturing from acidic to neutral conditions. Also, during biological action, the particles undergo an environmental pH change from about neutral in circulation to acidic conditions on endosomal uptake and processing. The observation of pH-dependent structural changes constitutes an important extension to the insight that can be given by the fluorescence-based assay. It provides direct structural information of the overall mRNA/lipid stacks instead of only the accessible interfacial moieties and is not dependent on environmental settings such as buffer choice. These structural parameters are relevant for cellular processing (e.g., endosomal uptake and release) and stability perspectives (e.g., drug substance and lipid integrity). As a further criterion, which has not been extensively considered so far, we propose to analyze the Porod exponent in the low-q region and to determine the (surface) fractal dimension. The interfacial molecular conformation appears to be important for cellular uptake and endosomal release processes and thus affects drug product activity. Following these approaches, we were able to identify certain structural features that varied with the relative activity of the four ionizable model lipids:

i. The more potent lipids exhibited a higher perpendicular packing density of the mRNA-lipid complexes than those with lower potency. The higher packing density was maintained when the pH was increased to neutral levels, as it occurs following intravenous administration in the systemic circulation. This is envisaged to provide better protection against the degradation of the particles within the circulation. Considering that the mRNA-lipid Bragg peak was maintained over the entire pH range tested, it demonstrated the general stability of the complexes in varying pH environments during circulation after administration. However, it should be noted that circulation stability depends on additional variables such as shear forces and protein and membrane interactions.
ii. We found evidence for the coexistence of two different types of ordered material in the same LNP formulation. In fact, in standard LNP formulations, a relatively high excess of ionizable lipid relative to mRNA (N/P ratio > 4) is used. For reasons of charge balance, and supported by previous data [30] mRNA-lipid complexes inside the LNPs are expected to have an N/P ratio close to one. Therefore, we assume that the two patterns in the nanoparticles resulted from complexes with higher and lower (or no) amounts of mRNA inserted between the lipids. As in many LNP systems the excess lipid is important for activity, it appears helpful to gain more insight into the fraction having different structural organization inside the LNPs. It should be noted that several studies have reported the presence of LNPs with varying loads of RNA in a given formulation [53]. In this study, batch measurements averaging the signals from all types of present LNPs were performed, and the data did not allow for clear discrimination between these two options. Separation of different nanoparticle fractions before the SAXS measurement, such as by using AF4, can help to gain better insights into the individual properties of the different fractions in a product [28]. Such separation approaches will be helpful for better evaluation of the quality and activity of LNP formulations.
iii. We found a correlation between activity and the surface fractal dimension of the LNPs, a parameter that has not been widely considered by the community yet. Previously, when we observed higher transfection efficacy of MC3 compared to DODMA in human peripheral blood mononuclear cells (hPBMCs), we already found a higher surface fractal dimension for the more active formulations, particularly at acidic pH [31]. We hypothesize that the increased surface roughness may be favorable for interactions with the endosomal membrane, thereby promoting mechanisms of endosomal escape. Increased fractal dimensions may destabilize endosomal membranes within the phase where positive LNP charges and negative endosomal charges interact. Particles with rough interfaces or molecular moieties which loop away from the surface of the particles may reduce the energy barrier to rupture the (opposite) membrane compared to a particle with smooth interface. This could lead to higher permeability of the endosomal compartment. It will be worthwhile to investigate such membrane effects also in model membrane systems which allow quantitative assessment of the interactions (e.g., Atomic Force Microscopy, Surface Force Apparatus) and to correlate these results with activity.
iv. Some fundamental differences in the structural features of LNPs manufactured at N/P ratio < 1 compared to N/P ratio > 1 were evident. For formulations with an N/P ratio below 1, only a single type of internal organization was present. We conclude that mRNA/lipid complexes of defined stoichiometry had been formed (accounting for charge balance), coexisting with an excess of mRNA, which is not part of the particles and did not contribute to the scattering patterns obtained here. Higher order peaks were visible for the lipid complexed mRNA structure,

indicating inverted hexagonal phase, one of the paradigms in rational lipid synthesis for nucleic acid delivery.

v. The structural pK_a of the formulations determined by SAXS provides extended information compared to the traditional fluorescence-based approach. While the values for DODMA and MC3 were rather similar, ALC-0315 showed a lower SAXS-derived value, and DODAP showed a lower TNS assay-derived value.

vi. We identified a clear dependency of the N/P ratio on the structural pK_a value. The decrease in the pK_a with increasing N/P could be one reason for the high excess of ionizable lipid in current LNP products. This highlights that for developing new LNP formulations, the selection of ionizable lipid, lipid composition, and N/P ratio together contributes to the pH-dependent electrostatic properties of the particles. With a given lipid, the effective pK_a value of the particle can be fine-tuned by adjusting the N/P ratio. Taking this into consideration, this can help to tailor mRNA LNP formulations for a given therapeutic use.

With this, a set of generally applicable tools can be provided that allow us to evaluate and compare product quality and to accelerate the development of tailored LNP formulations for future applications.

5. Conclusion

In this study, model LNP compositions were investigated with SAXS measurements, and structural features were identified that correlated with transfection efficacy. The structural pH responsiveness for LNPs yielded in similar, but refined results, which more accurately display the actual in situ pH-dependent behavior of LNPs compared to the standard fluorescence-based assay for determination of nanoparticle pK_a. We found the structural pK_a value to systematically vary with N/P value, which introduces a further degree of freedom in LNP optimization. The optimal N/P values for active formulations may vary with ionizable lipids having different molecular pK_a values. High perpendicular packing density of the mRNA/lipid stacks and a high increase in surface roughness (fractal dimension) in response to lowering pH were characteristic of the more potent ionizable lipids. Overall, concise structural investigations by SAXS can be helpful in rational LNP design. Structural features characteristic of potent lipid excipients and LNPs can be identified, and general structure-function correlations for mRNA LNPs, a versatile drug delivery system for various therapeutic targets, can be derived.

CRediT authorship contribution statement

Christoph Wilhelmy: Writing – original draft, Visualization, Methodology, Investigation, Formal analysis. **Lukas Uebbing:** Writing – review & editing, Methodology, Investigation. **Bastian Kolb:** Writing – review & editing, Investigation. **Melissa A. Graewert:** Writing – review & editing, Investigation. **Thomas Nawroth:** Writing – review & editing. **Heinrich Haas:** Writing – original draft, Supervision, Conceptualization. **Peter Langguth:** Writing – review & editing, Supervision, Project administration, Funding acquisition, Conceptualization.

Funding sources

This work was funded by the „Deutsche Forschungsgemeinschaft (DFG)“, Sonderforschungsbereich 1066, and the “Bundesministerium für Bildung und Forschung (BMBF)“, grant number 05K22UM3.

Declaration of competing interest

All authors declare no competing interests.

Acknowledgements

We would like to thank Lipoid GmbH for donating some of the lipids, namely DOPE. The synchrotron SAXS data was collected at beamline P12 operated by EMBL Hamburg at the PETRA III storage ring (DESY, Hamburg, Germany).

Appendix A. Supplementary data

Supplementary data to this article can be found online at https://doi.org/10.1016/j.jconrel.2025.113848.

Data availability

Data will be made available on request.

References

[1] U. Sahin, K. Karikó, Ö. Türeci, mRNA-based therapeutics—developing a new class of drugs, Nat. Rev. Drug Discov. 13 (2014) 759–780, https://doi.org/10.1038/nrd4278.

[2] L.M. Kranz, M. Diken, H. Haas, S. Kreiter, C. Loquai, K.C. Reuter, M. Meng, D. Fritz, F. Vascotto, H. Hefesha, et al., Systemic RNA delivery to dendritic cells exploits antiviral defence for cancer immunotherapy, Nature 534 (2016) 396–401, https://doi.org/10.1038/nature18300.

[3] S. Chen, X. Huang, Y. Xue, E. Álvarez-Benedicto, Y. Shi, W. Chen, S. Koo, D. J. Siegwart, Y. Dong, W. Tao, Nanotechnology-based mRNA vaccines, Nat Rev Methods Primers 3 (2023), https://doi.org/10.1038/s43586-023-00246-7.

[4] J.D. Beck, D. Reidenbach, N. Salomon, U. Sahin, Ö. Türeci, M. Vormehr, L. M. Kranz, mRNA therapeutics in cancer immunotherapy, Mol. Cancer 20 (2021) 69, https://doi.org/10.1186/s12943-021-01348-0.

[5] N. Pardi, S. Tuyishime, H. Muramatsu, K. Kariko, B.L. Mui, Y.K. Tam, T.D. Madden, M.J. Hope, D. Weissman, Expression kinetics of nucleoside-modified mRNA delivered in lipid nanoparticles to mice by various routes, J. Control. Release 217 (2015) 345–351, https://doi.org/10.1016/j.jconrel.2015.08.007.

[6] A. Akinc, M.A. Maier, M. Manoharan, K. Fitzgerald, M. Jayaraman, S. Barros, S. Ansell, X. Du, M.J. Hope, T.D. Madden, et al., The Onpattro story and the clinical translation of nanomedicines containing nucleic acid-based drugs, Nat. Nanotechnol. 14 (2019) 1084–1087, https://doi.org/10.1038/s41565-019-0591-y.

[7] E.E. Walsh, R.W. Frenck, A.R. Falsey, N. Kitchin, J. Absalon, A. Gurtman, S. Lockhart, K. Neuzil, M.J. Mulligan, R. Bailey, et al., Safety and immunogenicity of two RNA-based Covid-19 vaccine candidates, N. Engl. J. Med. 383 (2020) 2439–2450, https://doi.org/10.1056/NEJMoa2027906.

[8] C. Hald Albertsen, J.A. Kulkarni, D. Witzigmann, M. Lind, K. Petersson, J. B. Simonsen, The role of lipid components in lipid nanoparticles for vaccines and gene therapy, Adv. Drug Deliv. Rev. 188 (2022) 114416, https://doi.org/10.1016/j.addr.2022.114416.

[9] L. Schoenmaker, D. Witzigmann, J.A. Kulkarni, R. Verbeke, G. Kersten, W. Jiskoot, D.J.A. Crommelin, mRNA-lipid nanoparticle COVID-19 vaccines: structure and stability, Int. J. Pharm. 601 (2021) 120586, https://doi.org/10.1016/j.ijpharm.2021.120586.

[10] P. Patel, N.M. Ibrahim, K. Cheng, The importance of apparent pKa in the development of nanoparticles encapsulating siRNA and mRNA, Trends Pharmacol. Sci. 42 (2021) 448–460, https://doi.org/10.1016/j.tips.2021.03.002.

[11] H. Yu, J. Iscaro, B. Dyett, Y. Zhang, S. Seibt, N. Martinez, J. White, C.J. Drummond, S. Bozinovski, J. Zhai, Inverse cubic and hexagonal Mesophase evolution within Ionizable lipid nanoparticles correlates with mRNA transfection in macrophages, J. Am. Chem. Soc. 145 (2023) 24765–24774, https://doi.org/10.1021/jacs.3c08729.

[12] J. Philipp, A. Dabkowska, A. Reiser, K. Frank, R. Krzysztoń, C. Brummer, B. Nickel, C.E. Blanchet, A. Sudarsan, M. Ibrahim, et al., pH-dependent structural transitions in cationic ionizable lipid mesophases are critical for lipid nanoparticle function, Proc. Natl. Acad. Sci. U. S. A. 120 (2023) e2310491120, https://doi.org/10.1073/pnas.2310491120.

[13] Q. Cheng, T. Wei, L. Farbiak, L.T. Johnson, S.A. Dilliard, D.J. Siegwart, Selective organ targeting (SORT) nanoparticles for tissue-specific mRNA delivery and CRISPR-Cas gene editing, Nat. Nanotechnol. 15 (2020) 313–320, https://doi.org/10.1038/s41565-020-0669-6.

[14] Y. Xu, A. Golubovic, S. Xu, A. Pan, B. Li, Rational design and combinatorial chemistry of ionizable lipids for RNA delivery, J. Mater. Chem. B 11 (2023) 6527–6539, https://doi.org/10.1039/D3TB00649B.

[15] G. Tilstra, J. Couture-Senécal, Y.M.A. Lau, A.M. Manning, D.S.M. Wong, W. W. Janaeska, T.A. Wuraola, J. Pang, O.F. Khan, Iterative Design of Ionizable Lipids for intramuscular mRNA delivery, J. Am. Chem. Soc. 145 (2023) 2294–2304, https://doi.org/10.1021/jacs.2c10670.

[16] M. Jayaraman, S.M. Ansell, B.L. Mui, Y.K. Tam, J. Chen, X. Du, D. Butler, L. Eltepu, S. Matsuda, J.K. Narayanannair, et al., Maximizing the potency of siRNA lipid nanoparticles for hepatic gene silencing in vivo, Angew. Chem. Int. Ed. Engl. 51 (2012) 8529–8533, https://doi.org/10.1002/anie.201203263.

[17] C. Azevedo, M.H. Macedo, B. Sarmento, Strategies for the enhanced intracellular delivery of nanomaterials, Drug Discov. Today 23 (2018) 944–959, https://doi.org/10.1016/j.drudis.2017.08.011.
[18] M.J. Carrasco, S. Alishetty, M.-G. Alameh, H. Said, L. Wright, M. Paige, O. Soliman, D. Weissman, T.E. Cleveland, A. Grishaev, et al., Ionization and structural properties of mRNA lipid nanoparticles influence expression in intramuscular and intravascular administration, Commun. Biol. 4 (2021) 956, https://doi.org/10.1038/s42003-021-02441-2.
[19] K.J. Hassett, K.E. Benenato, E. Jacquinet, A. Lee, A. Woods, O. Yuzhakov, S. Himansu, J. Deterling, B.M. Geilich, T. Ketova, et al., Optimization of lipid nanoparticles for intramuscular administration of mRNA vaccines, Mol. Ther. Nucleic Acids 15 (2019) 1–11, https://doi.org/10.1016/j.omtn.2019.01.013.
[20] M.D. Buschmann, M.J. Carrasco, S. Alishetty, M. Paige, M.G. Alameh, D. Weissman, Nanomaterial delivery systems for mRNA vaccines, Vaccines (Basel) 9 (2021), https://doi.org/10.3390/vaccines9010065.
[21] S.L. Rybak, R.F. Murphy, Primary cell cultures from murine kidney and heart differ in endosomal pH, J. Cell. Physiol. 176 (1998) 216–222, https://doi.org/10.1002/(SICI)1097-4652(199807)176:1<216:AID-JCP23>3.0.CO;2-3.
[22] S.A. Dilliard, Q. Cheng, D.J. Siegwart, On the mechanism of tissue-specific mRNA delivery by selective organ targeting nanoparticles, Proc. Natl. Acad. Sci. U. S. A. 118 (2021), https://doi.org/10.1073/pnas.2109256118.
[23] S.S. Nogueira, E. Samaridou, J. Simon, S. Frank, M. Beck-Broichsitter, A. Mehta, Analytical techniques for the characterization of nanoparticles for mRNA delivery, Eur. J. Pharm. Biopharm. 198 (2024) 114235, https://doi.org/10.1016/j.ejpb.2024.114235.
[24] N.B. Hamilton, S. Arns, M. Shelley, I. Bechis, J.C. Shelley, Calculating apparent pKa values of Ionizable lipids in lipid nanoparticles, Mol. Pharm. (2024), https://doi.org/10.1021/acs.molpharmaceut.4c00426.
[25] M.F.W. Trollmann, R.A. Böckmann, mRNA lipid nanoparticle phase transition, Biophys. J. 121 (2022) 3927–3939, https://doi.org/10.1016/j.bpj.2022.08.037.
[26] L. Uebbing, A. Ziller, C. Siewert, M.A. Schroer, C.E. Blanchet, D.I. Svergun, S. Ramishetti, D. Peer, U. Sahin, H. Haas, et al., Investigation of pH-responsiveness inside lipid nanoparticles for parenteral mRNA application using small-angle X-ray scattering, Langmuir 36 (2020) 13331–13341, https://doi.org/10.1021/acs.langmuir.0c02446.
[27] C.D. Siewert, H. Haas, V. Cornet, S.S. Nogueira, T. Nawroth, L. Uebbing, A. Ziller, J. Al-Gousous, A. Radulescu, M.A. Schroer, et al., Hybrid biopolymer and lipid nanoparticles with improved transfection efficacy for mRNA, Cells 9 (2020), https://doi.org/10.3390/cells9092034.
[28] M.A. Graewert, C. Wilhelmy, T. Bacic, J. Schumacher, C. Blanchet, F. Meier, R. Drexel, R. Welz, B. Kolb, K. Bartels, et al., Quantitative size-resolved characterization of mRNA nanoparticles by in-line coupling of asymmetrical-flow field-flow fractionation with small angle X-ray scattering, Sci. Rep. 13 (2023) 15764, https://doi.org/10.1038/s41598-023-42274-z.
[29] S.S. Nogueira, A. Schlegel, K. Maxeiner, B. Weber, M. Barz, M.A. Schroer, C. E. Blanchet, D.I. Svergun, S. Ramishetti, D. Peer, et al., Polysarcosine-functionalized lipid nanoparticles for therapeutic mRNA delivery, ACS Appl. Nano Mater. 3 (2020) 10634–10645, https://doi.org/10.1021/acsanm.0c01834.
[30] A. Ziller, S.S. Nogueira, E. Hühn, S.S. Funari, G. Brezesinski, H. Hartmann, U. Sahin, H. Haas, P. Langguth, Incorporation of mRNA in lamellar lipid matrices for parenteral administration, Mol. Pharm. 15 (2018) 642–651, https://doi.org/10.1021/acs.molpharmaceut.7b01022.
[31] C. Wilhelmy, I.S. Keil, L. Uebbing, M.A. Schroer, D. Franke, T. Nawroth, M. Barz, U. Sahin, H. Haas, M. Diken, et al., Polysarcosine-functionalized mRNA lipid nanoparticles tailored for immunotherapy, Pharmaceutics 15 (2023), https://doi.org/10.3390/pharmaceutics15082068.
[32] D. Bi, C. Wilhelmy, D. Unthan, I.S. Keil, B. Zhao, B. Kolb, R.I. Koning, M. A. Graewert, B. Wouters, R. Zwier, et al., On the influence of fabrication methods and materials for mrna-lnp production: from size and morphology to internal structure and mrna delivery performance in vitro and in vivo, Adv. Healthc. Mater. (2024), https://doi.org/10.1002/adhm.202401252 e2401252.
[33] B. Binici, Z. Rattray, A. Zinger, Y. Perrie, Exploring the impact of commonly used ionizable and pegylated lipids on mRNA-LNPs: a combined in vitro and preclinical perspective, J. Control. Release 377 (2025) 162–173, https://doi.org/10.1016/j.jconrel.2024.11.010.
[34] O. Escalona-Rayo, Y. Zeng, R.A. Knol, T.J.F. Kock, D. Aschmann, B. Slütter, A. Kros, In vitro and in vivo evaluation of clinically-approved ionizable cationic lipids shows divergent results between mRNA transfection and vaccine efficacy, Biomed. Pharmacother. 165 (2023) 115065, https://doi.org/10.1016/j.biopha.2023.115065.
[35] C.E. Blanchet, A. Spilotros, F. Schwemmer, M.A. Graewert, A. Kikhney, C. M. Jeffries, D. Franke, D. Mark, R. Zengerle, F. Cipriani, et al., Versatile sample environments and automation for biological solution X-ray scattering experiments at the P12 beamline (PETRA III, DESY), J. Appl. Cryst. 48 (2015) 431–443, https://doi.org/10.1107/S160057671500254X.
[36] A. Round, F. Felisaz, L. Fodinger, A. Gobbo, J. Huet, C. Villard, C.E. Blanchet, P. Pernot, S. McSweeney, M. Roessle, et al., BioSAXS sample changer: a robotic sample changer for rapid and reliable high-throughput X-ray solution scattering experiments, Acta Crystallogr. D Biol. Crystallogr. 71 (2015) 67–75, https://doi.org/10.1107/S1399004714026959.
[37] B. Romeis, Taschenbuch der mikroskopischen Technik, De Gruyter, 1943. ISBN 9783486764369.
[38] K. Manalastas-Cantos, P.V. Konarev, N.R. Hajizadeh, A.G. Kikhney, M. V. Petoukhov, D.S. Molodenskiy, A. Panjkovich, H.D.T. Mertens, A. Gruzinov, C. Borges, et al., ATSAS 3.0: expanded functionality and new tools for small-angle scattering data analysis, J. Appl. Cryst. 54 (2021) 343–355, https://doi.org/10.1107/S1600576720013412.
[39] G. Porod, Die Röntgenkleinwinkelstreuung von dichtgepackten kolloiden Systemen, Kolloid-Zeitschrift 124 (1951) 83–114, https://doi.org/10.1007/BF01512792.
[40] H.D. Bale, P.W. Schmidt, Small-angle X-ray-scattering investigation of submicroscopic porosity with fractal properties, Phys. Rev. Lett. 53 (1984) 596–599, https://doi.org/10.1103/PhysRevLett.53.596.
[41] G. Beaucage, Small-angle scattering from polymeric mass fractals of arbitrary mass-fractal dimension, J. Appl. Cryst. 29 (1996) 134–146, https://doi.org/10.1107/S0021889895011605.
[42] W.H. Bragg, William L. Bragg, The reflection of X-rays by crystals, Proc. R. Soc. Lond. A 88 (1913) 428–438, https://doi.org/10.1098/rspa.1913.0040.
[43] Second completely revised and greatly enlarged edition, in: J.W.G. Goodby, P. J. Collings, T. Kato, C. Tschierske, H.F. Gleeson, E.P. Raynes (Eds.), Handbook of Liquid Crystals, Wiley-VCH, Weinheim, 2014. ISBN 9783527671403.
[44] J. Heyes, L. Palmer, K. Bremner, I. MacLachlan, Cationic lipid saturation influences intracellular delivery of encapsulated nucleic acids, J. Control. Release 107 (2005) 276–287, https://doi.org/10.1016/j.jconrel.2005.06.014.
[45] T.F. Martens, K. Remaut, J. Demeester, S.C. Smedt, de; Braeckmans, K., Intracellular delivery of nanomaterials: how to catch endosomal escape in the act, Nano Today 9 (2014) 344–364, https://doi.org/10.1016/j.nantod.2014.04.011.
[46] A.-M. Börjesdotter, H. Bolinsson, T. Dagø, F. Herranz-Trillo, U.C. Palmiero, H. Schagerlöf, L. Nilsson, Lipid nanoparticle properties explored using online asymmetric flow field-flow fractionation coupled with small angle X-ray scattering: beyond average characterisation, Int. J. Pharm. 668 (2025) 124940, https://doi.org/10.1016/j.ijpharm.2024.124940.
[47] S. Ciccariello, J. Goodisman, H. Brumberger, On the Porod law, J. Appl. Cryst. 21 (1988) 117–128, https://doi.org/10.1107/S0021889887010409.
[48] F. Sebastiani, M. Yanez Arteta, M. Lerche, L. Porcar, C. Lang, R.A. Bragg, C. S. Elmore, V.R. Krishnamurthy, R.A. Russell, T. Darwish, et al., Apolipoprotein E binding drives structural and compositional rearrangement of mRNA-containing lipid nanoparticles, ACS Nano 15 (2021) 6709–6722, https://doi.org/10.1021/acsnano.0c10064.
[49] V. Nele, V. Campani, S. Alia Moosavian, G. de Rosa, Lipid nanoparticles for RNA delivery: self-assembling vs driven-assembling strategies, Adv. Drug Deliv. Rev. 208 (2024) 115291, https://doi.org/10.1016/j.addr.2024.115291.
[50] J.M. Seddon, Structure of the inverted hexagonal (HII) phase, and non-lamellar phase transitions of lipids, Biochim. Biophys. Acta 1031 (1990) 1–69, https://doi.org/10.1016/0304-4157(90)90002-T.
[51] I. Koltover, T. Salditt, J.O. Rädler, C.R. Safinya, An inverted hexagonal phase of cationic liposome-DNA complexes related to DNA release and delivery, Science 281 (1998) 78–81, https://doi.org/10.1126/science.281.5373.78.
[52] X. Cheng, R.J. Lee, The role of helper lipids in lipid nanoparticles (LNPs) designed for oligonucleotide delivery, Adv. Drug Deliv. Rev. 99 (2016) 129–137, https://doi.org/10.1016/j.addr.2016.01.022.
[53] J.B. Simonsen, A perspective on bleb and empty LNP structures, J. Control. Release 373 (2024) 952–961, https://doi.org/10.1016/j.jconrel.2024.07.046.